Paper 094

TRIMMED ACTUATOR DISK MODELING FOR HELICOPTER ROTOR

M. Biava[1], M. Valentini[2], L. Vigevano[2]

[1] AWPARC, Milano, Italy [2] Dipartimento di Scienze e Tecnologie Aerospaziali - Politecnico di Milano, Via La Masa 34, 20156 Milano, Italy

Abstract

We present a method to compute the flow field around a trimmed helicopter rotor using an Actuator Disc (AD) model where the source distribution and the orientation of the disc with respect to the shaft axis are adapted during the simulation, in order to meet the prescribed trim state. In a standard AD simulation the momentum source is assigned *a priori* or is computed with a simplified linear trim procedure. In this work the source distribution is provided by a multi-body trimmed rotor simulation which fully accounts for the blade dynamics, loosely coupled with a CFD solver. Results achieved with this simplified rotor model compare positively with experimental results, thus representing a good compromise between the quality of results and the computational effort.

1 Introduction

In the last decades, quite a number of Actuator Disk (AD) or Actuator Line (AL) models, coupled with CFD flow solvers, have been developed to investigate rotorcraft interference effects in a computationally efficient way. In fact, these methods do not require to generate grids for the individual rotor blades, reducing the cost in term of operation and grid development and still allowing an estimate of the rotor flow and wake effects.

The AD concept, first considered for propeller-wing interactional flow by Whitfield and Jameson[1], introduces the assumption of time-averaged flow and represents the rotor as an infinitely thin disk which carries discontinuities of flow properties, using source terms in the momentum and energy equations or enforcing a pressure jump on the disk boundary. Sectional blade loads are usually computed with the Blade Element Theory (BET), with the gas velocity provided by the CFD flow simulation. In its unsteady counterpart, the AL model, the rotating blades are projected into the disk and their traces act similarly on the fluid in a time-dependent manner.

A classification of previous AD/CFD coupled models applied to helicopter rotor flows is not a straightforward task, because of the different combination of model elements which may be observed. Besides the distinction among steady AD[2–13] and unsteady AL[13–16] models, Le Chuiton[2] analyzed in detail the different implementations of the AD model in terms of enforcement of boundary conditions[3–6] or addition of source terms[7–12], concluding that the latter option was preferable for robustness. O'Brien and Smith[10] addressed the effect of different assigned disk load shapes, ranging from a constant load to that computed with the BET. In addition, other features of the model may be put into evidence: the type of governing equations employed by the CFD solver, either Euler[5,6,13], incompressible Reynolds-Averaged Navier–Stokes (RANS)[4,7,8] or Large Eddy Simulation (LES)[16], thin-layer RANS[3,14,15] or fully compressible RANS[6,10–12]; the type of coupling between AD model and CFD flow calculation, which ranges from an assigned load, either constant, linear, supplied by an external program or computed with BET and an assigned blade kinematics[2,7–11,13,16], to a loosely coupled load obtained with a simplified linear trimming procedure[3–6,12,14,15]. Assigned blade flapping with prescribed kinematics is explicitly accounted only by Zori and Rajagopalan[8] .

None of the preceding methods accounts for the blade dynamics in the rotor trimming procedure. The goal of the present work has been to develop a method to compute the trim commands for an helicopter rotor using an AD model wich fully accounts for the blade dynamics and where the source distribution and the orientation of the disk with respect to the shaft axis are adapted during the simulation, in order to meet the prescribed trim state. Blade loads are computed with the standard BET with gas velocity provided by the CFD solution, while blade dynamics is represented by a multi-body description of the rotor using the *MBDyn* code[17]. The trimmed AD model has been embedded in *ROSITA*[18], a compressible RANS solver developed at Politecnico di Milano. *ROSITA* uses a system of overset grids (Chimera), which allow to give the actuator disc grid the same orientation as the rotor tip path plane without the need of remeshing.

The proposed method is validated by simulating a model rotor during experimental tests in the open test section of the Politecnico di Milano (PoliMi) large wind tunnel, a flow configuration where it is important to account for the influence of the wind tunnel jet deviation on the rotor operating conditions. The trimmed AD results are compared with experimental data in terms of control angles and global rotor loads. Furthermore, a portion of the velocity field downstream of the rotor itself is analyzed using two-component PIV measurements.

The structure of the paper is as follows. Section 2 summarizes the main characteristic of the CFD and CSD solvers. Sections 3 and 4 describe the proposed model, which is validated against experimental and numerical results in section 5. Some conclusions are drawn in the last section.

2 The CFD/CSD solvers

2.1 The flow solver *ROSITA*

The *ROSITA* flow solver[18,19] numerically integrates the RANS equations, coupled with the one-equation turbulence model of Spalart–Allmaras[20], in systems of moving, overset, multi-block grids. The equations are discretized in space by means of a cell-centred finite-volume implementation of the Roe's scheme[21]. Second order accuracy is obtained through the use of MUSCL extrapolation supplemented with a modified version of the Van Albada limiter introduced by Venkatakrishnan[22]. The viscous terms are computed by the application of the Gauss theorem and using a cell-centred discretization scheme. Time advancement is carried out with a dual-time formulation[23], employing a 2$^{\text{nd}}$ order backward differentiation formula to approximate the time derivative and a fully unfactored implicit scheme in pseudo-time. The generalized conjugate gradient (GCG), in conjunction with a block incomplete lower-upper preconditioner, is used to solve the resulting linear system.

To compute the low speed, steady flows considered in the present work, Turkel's[24] low Mach preconditioner has been employed.

The connectivity between the (possibly moving) component grids is computed by means of the Chimera technique. The approach adopted in *ROSITA* is derived from that originally proposed by Chesshire and Henshaw[25], with modifications to further improve robustness and performance.

2.2 The multi-body solver *MBDyn*

MBDyn is a free general-purpose multi-body analysis software[17]. It is mainly intended for structural dynamics simulations, although it provides some intrinsic multidisciplinary analysis capabilities. It is mildly oriented towards the analysis of rotorcraft systems through the availability of simplified built-in rotor blade aerodynamics. The analysis is based on the integration in time of the Newton-Euler equations of motion of a set of discrete bodies, subjected to configuration-dependent forces that model deformability and aerodynamic loads, and connected by kinematic constraints expressed using the Lagrangian multipliers formalism[26]. The deformable components library consists in lumped components, kinematically exact and composite-ready nonlinear beam elements suitable for the modeling of rotor blades, and component mode synthesis elements, mainly used for the modeling of non-rotating components, like the airframe. The modularity of the formulation eased the coupling with the *ROSITA* CFD solver. The rotor trim algorithm used in conjunction with BET is derived from Peters *et al*[27].

3 The rotor model

The actuator disk approximates the forces that the rotor blades apply to the air flow over a disk having the same diameter of the rotor. In *ROSITA* the actuator disk is implemented as a non uniform source distribution in a single layer of cells of a cylindrical grid (see figure 1).

In order to define the actuator disk source terms, we start recalling the non-dimensionalized Navier-Stokes equations in integral form applied to a control volume $\mathcal{V}_{ijk}$ and surface boundary $\mathcal{S}_{ijk}$:

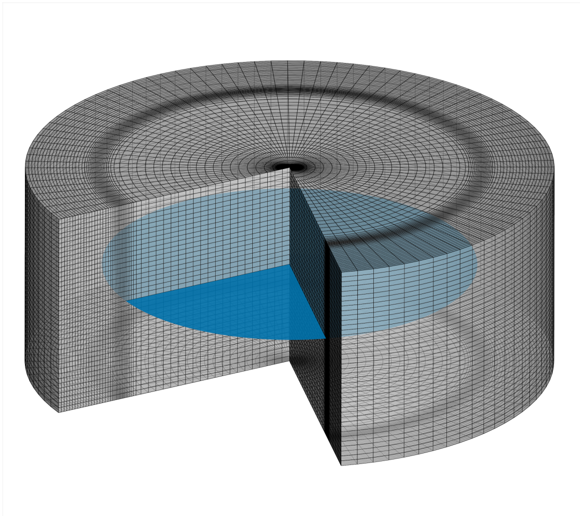

Figure 1: Actuator disk grid. The highlighted region denotes the layer of cells where the actuator disk sources are introduced.

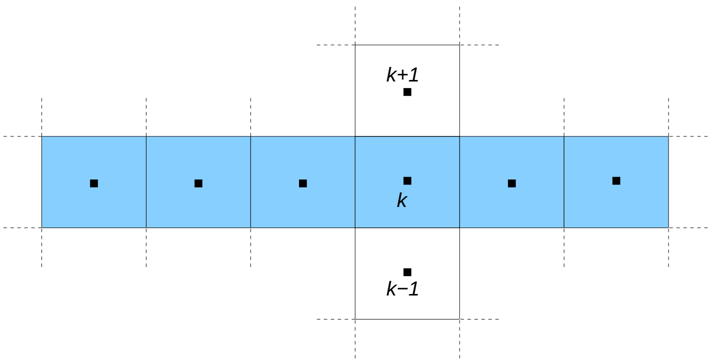

Figure 2: Schematic representation of the actuator disk cell layer.

$$\frac{\partial}{\partial t}\oint_{\mathcal{V}_{ijk}} \boldsymbol{W}\, d\mathcal{V} + \int_{\mathcal{S}_{ijk}} \left(\boldsymbol{F_c}\cdot\boldsymbol{n} - \boldsymbol{v}\cdot\boldsymbol{n}\boldsymbol{W}\right) d\mathcal{S} - \int_{\mathcal{S}_{ijk}} \boldsymbol{F_d}\cdot\boldsymbol{n}\; d\mathcal{S} = \oint_{\mathcal{V}_{ijk}} \boldsymbol{S}\, d\mathcal{V},$$

where $\boldsymbol{W} = [\rho, \rho u, \rho v, \rho w, \rho E]^T$ denotes the vector of conservative variables, $\boldsymbol{F_c} = \boldsymbol{F_c}(\boldsymbol{W})$ is the convective flux tensor, $\boldsymbol{F_d} = \boldsymbol{F_d}(\boldsymbol{W}, \boldsymbol{\nabla W})$ is the diffusive flux tensor, $\boldsymbol{S} = \boldsymbol{S}(\boldsymbol{W})$ represents the source term due to the movement of the relative frame, $\boldsymbol{v}$ is the sum of the entrainment velocity vector and the grid deformation velocity vector, $\mathcal{V}$ is the cell volume and $\mathcal{S}$ is the cell surface, with unit normal $\boldsymbol{n}$.

The space discretization leads to a system of ordinary equations for the rate of change of the conservative flow variables associated to the centres of the control volumes. The system then reads:

$$\frac{d}{dt}\left(\mathcal{V}\boldsymbol{W}\right)_{ijk} + \boldsymbol{R}_{ijk} = 0, \qquad (1)$$

where $\boldsymbol{R}_{ijk}$ represents the flux balance across $\mathcal{S}_{ijk}$, which can be written as:

$$\boldsymbol{R}_{ijk} = (\boldsymbol{Q_c})_{ijk} - (\boldsymbol{Q_d})_{ijk} - \boldsymbol{S}_{ijk},$$

where $(\boldsymbol{Q_d})_{ijk}$ is the diffusive flux balance and $(\boldsymbol{Q_c})_{ijk}$ is the convective flux balance (convective and pressure effects).

Equations (1) are solved in *ROSITA* using a dual-time formulation with implicit pseudo-time discretization. At each pseudo time step Δt^*_{ijk} the variation $\Delta\boldsymbol{W}_{ijk} = \boldsymbol{W}^{m+1}_{ijk} - \boldsymbol{W}^{m}_{ijk}$ of the conservative variables is given by the solution of the following linear system:

$$\left[\left(\frac{\mathcal{V}^{n+1}_{ijk}}{\Delta t^*_{ijk}} + \frac{3\mathcal{V}^{n+1}_{ijk}}{2\Delta t}\right)\boldsymbol{I} + \frac{\partial \boldsymbol{R}^m_{ijk}}{\partial \boldsymbol{W}}\right]\Delta\boldsymbol{W}_{ijk} = -\boldsymbol{R}^*(\boldsymbol{W}^m_{ijk}),$$

where n is the real time step index and m is the pseudo time step index. The term $\boldsymbol{R}^*(\boldsymbol{W})_{ijk}$ stands for the unsteady residual:

$$\boldsymbol{R}^*(\boldsymbol{W}_{ijk}) = \frac{3\mathcal{V}^{n+1}_{ijk}\boldsymbol{W}_{ijk} - 4\left(\mathcal{V}\boldsymbol{W}\right)^n_{ijk} + 2\left(\mathcal{V}\boldsymbol{W}\right)^{n-1}_{ijk}}{2\Delta t} + \boldsymbol{R}(\boldsymbol{W}_{ijk}) \qquad (2)$$

and the corresponding Jacobian is

$$\frac{\partial \boldsymbol{R}^m_{ijk}}{\partial \boldsymbol{W}} = \frac{\partial (\boldsymbol{Q_c})^m_{ijk}}{\partial \boldsymbol{W}} - \frac{\partial (\boldsymbol{Q_d})^m_{ijk}}{\partial \boldsymbol{W}} - \frac{\partial \boldsymbol{S}^m_{ijk}}{\partial \boldsymbol{W}}. \qquad (3)$$

Suppose now to have a force (per unit area) distribution $\boldsymbol{f}_{ijk} = (f_x, f_y, f_z)$ over the actuator disk cell layer. This distribution may be prescribed or computed using BET. The associated momentum and energy source enter as an additional term in the definition of the unsteady residual (2) and we denote it as $\boldsymbol{S}_{\mathrm{ad},ijk}$. Since it is assumed in the code that the actuator disk source layer is a fixed k-plane of the grid (see figure 2) the source term can be written as:

$$\boldsymbol{S}_{\mathrm{ad},ijk} = \begin{bmatrix} 0 \\ f_x \\ f_y \\ f_z \\ \boldsymbol{f}_{ijk}\cdot\dfrac{(\rho\boldsymbol{v})^*_{ijk}}{\rho^*_{ijk}} \end{bmatrix},$$

where

$$\rho^*_{ijk} = \frac{1}{2}\left[\rho_{ij\,k-1} + \rho_{ij\,k+1}\right],$$

$$(\rho\boldsymbol{v})^*_{ijk} = \frac{1}{2}\left[(\rho\boldsymbol{v})_{ij\,k-1} + (\rho\boldsymbol{v})_{ij\,k+1}\right].$$

Note that the density and the momentum of the fluid at the cell (i,j,k) of the actuator disk are computed as the average of the corresponding quantities in the two adiacent cells $(i,j,k-1)$ and $(i,j,k+1)$, without considering the cell where the source is introduced. The reason is that pressure and velocity peaks are observed in correspondence of the actuator disk cell layer due to the local action of the source term.

For the implicit dual-time method the Jacobians of the source term with respect to $\boldsymbol{W}_{ij\,k-1}$ and to $\boldsymbol{W}_{ij\,k+1}$ are also needed, and must be accounted as additional terms in the right hand side of equation (3). They can be written as:

$$\frac{\partial \boldsymbol{S}_{\mathrm{ad},ijk}}{\partial \boldsymbol{W}_{ij\,k\pm1}} = \begin{bmatrix} 0 & & \dots & & 0 \\ \vdots & & & & \vdots \\ 0 & & \dots & & 0 \\ -\boldsymbol{f}_{ijk}\cdot\dfrac{(\rho\boldsymbol{v})^*_{ijk}}{2\,(\rho^*_{ijk})^2} & \dfrac{f_x}{2\rho^*_{ijk}} & \dfrac{f_y}{2\rho^*_{ijk}} & \dfrac{f_z}{2\rho^*_{ijk}} & 0 \end{bmatrix}.$$

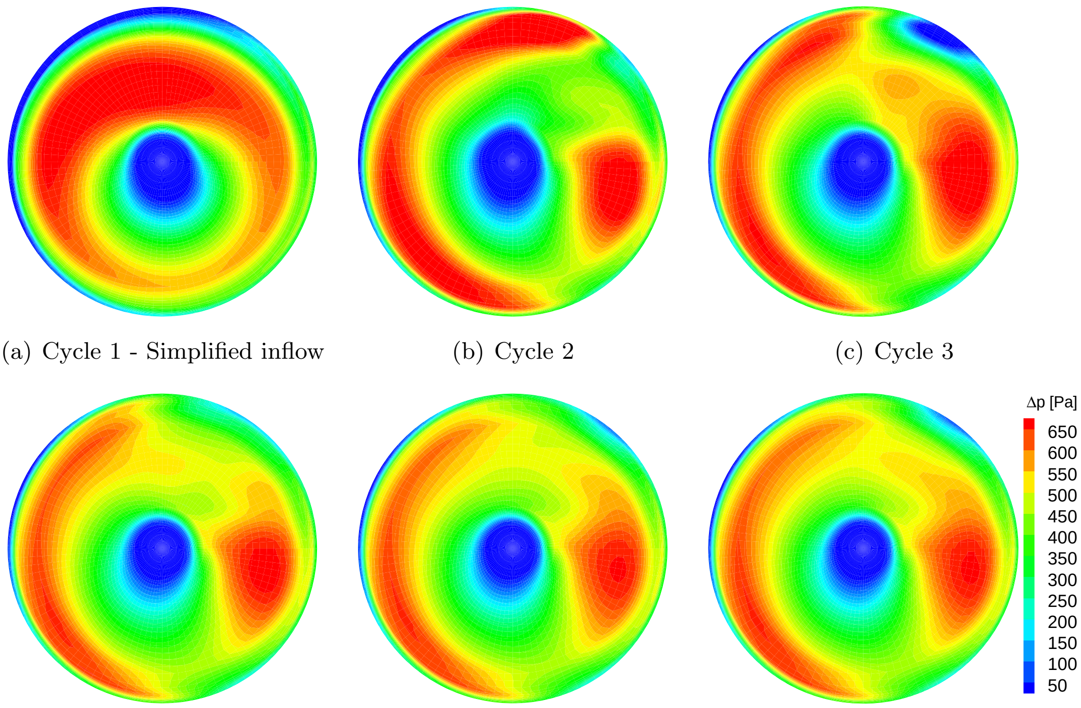

(a) Cycle 1 - Simplified inflow (b) Cycle 2 (c) Cycle 3

(d) Cycle 4 (e) Cycle 5 (f) Cycle 6

Figure 3: Actuator disk load distribution evolution over the coupling cycles.

Test case	M_{tip}	Target C_T/σ	V_{wt} [m/s]	α_s [deg]
TC1	0.6226	0.1	10	0°
TC2	0.6226	0.1	15	0°
TC3	0.6226	0.1	20	0°
TC4	0.6226	0.1	30	0°
TC5	0.6226	0.1	40	0°

Table 1: Selected test cases for the trimmed simulation of the 4-bladed AW rotor in the Politecnico di Milano large wind tunnel.

4 Coupling method

The proposed method computes the trim commands for an helicopter rotor using an AD model where the source distribution and the orientation of the disk with respect to the shaft axis are adapted during the simulation, in order to meet the prescribed trim state. The source distribution and the tip path plane orientation are obtained from a loose coupling between the CSD code *MBDyn* and the CFD code *ROSITA*. A multi-body trimmed rotor simulation is performed with *MBDyn*. The actuator disk is embedded in a child Chimera grid of the *ROSITA* simulation, which allows to give the AD grid the same orientation as the rotor tip path plane without the need of remeshing.

The coupling procedure works as follows.

(a) *MBDyn* computes an initial trim state using one of its embedded simple inflow models and provides a rotor map (a radial and azimuthal load distribution) and the disk orientation to *ROSITA*.

(b) *ROSITA* is then run until a steady inflow condition is reached at the disk surface, thus providing an updated inflow map to the CSD solver.

(c) *MBDyn* uses the CFD inflow map to compute a new trimmed solution and to find the updated load distribution on the rotor.

Points (b) and (c) are repeated until the variation of the rotor commands between to successive coupling cycles is below a prescribed tolerance. The coupling method has demonstrated to have a good convergence rate, in fact the solution becomes stable after about 5-10 cycles.

Since the CFD model takes into account the environment surrounding the rotor and its influence on the rotor inflow, the coupled method is able to compute the trimmed solution for both wind tunnel and free air conditions. More complex conditions can also be modeled, such as the presence of the helicopter fuselage.

As an example we consider the following test case: an isolated 4-bladed rotor in free air conditions, $V_{\text{inf}} = 30\,\text{m/s}$; the trim target is $C_T/\sigma = 0.1$, $\beta_{1,\text{s}} = 0$, $\beta_{1,\text{c}} = 0$. In figure 3 it is reported the AD load distribution for the first six *ROSITA*/*MBDyn* coupling cycles. As can be seen, the distribution has converged to a stable one after five cycles. The load distribution at the sixth iteration is far more representative of a real rotor with respect to the first, which is computed using the *MBDyn* embedded simplified inflow model. The iteration history of the Fourier components of the control and hinge angles (fig. 4) shows to have reached a converged state.

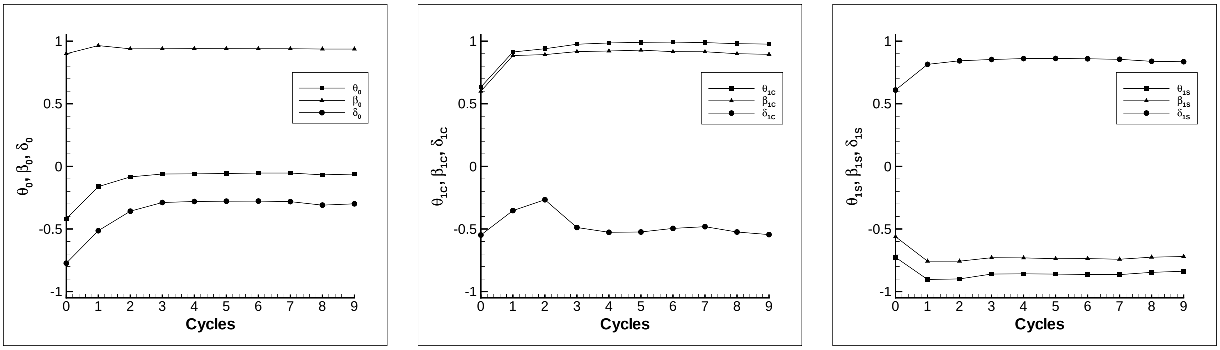

Figure 4: Normalized kinematic parameters evolution over the iteration cycles

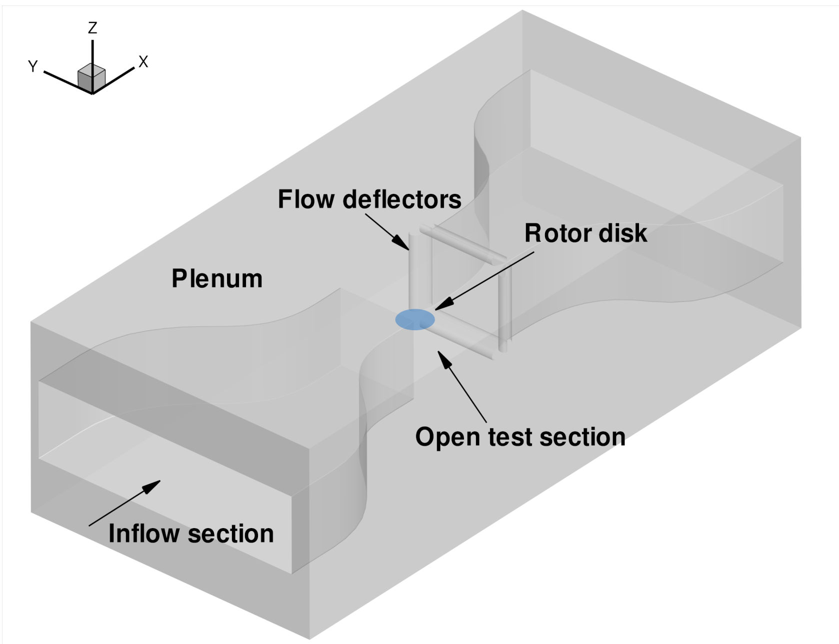

Figure 5: Numerical domain for the CFD computations.

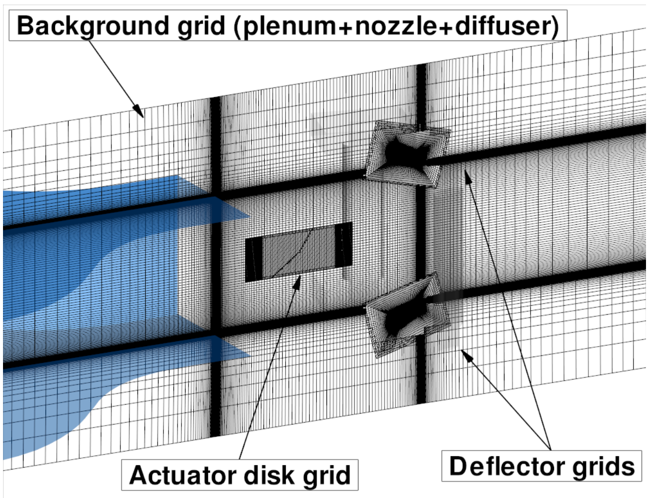

Figure 6: Numerical grid for the CFD computations.

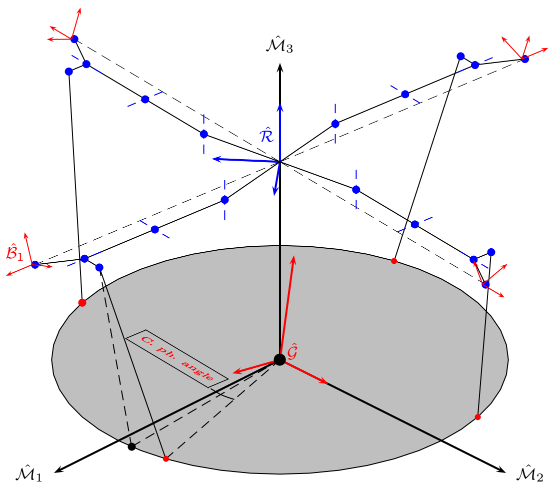

Figure 7: *MBDyn* model of the 4-bladed rotor hub.

5 Validation

To validate the coupled actuator disk model we made use of the experimental data gathered during the WITCH project, in which a model rotor was tested to investigate tunnel wall interference effects[28]. To this aim, a CFD model of the open test section of PoliMi large wind tunnel was implemented, which includes the test section itself and the whole surrounding chamber of the building that houses the wind tunnel circuit (see figure 5). The Chimera grid system consists of: a background mesh which represents the chamber containing part of the wind tunnel circuit and the open test section; four grids representing the flow deflectors placed at the beginning of the wind tunnel return circuit; a cylindrical mesh for the actuator disk. Figure 6 reports a slice of the computational mesh in the symmetry plane of the wind tunnel, where the different component grids can be clearly identified. In total the mesh counts about 13 million cells. The applied boundary conditions are: viscous wall boundary conditions on the wind tunnel walls; inviscid wall boundary conditions on the chamber walls; velocity inlet boundary conditions at the inflow section; pressure outlet boundary conditions at the outflow section.

The *MBDyn* model of the 4-bladed AW test rotor, employed for the multi-body computations, includes the description of a fully articulated hub, with swash plate and pitch links, hinges and blades. Several reference systems are utilized to represent the rotor components; figure 7 shows a sketch of the model, where the following reference systems are defined: the fixed inertial frame $\hat{\mathcal{G}}$, the shaft frame $\hat{\mathcal{M}}$, the rotating frame $\hat{\mathcal{R}}$ and the local blade frame $\hat{\mathcal{B}}$. The aerodynamic tables for the blade airfoils, used in BET, were computed with the *ROSITA* code for an average value of the ratio Re/M (Reynolds over Mach) of 2×10^6, which is the correct Re range for the model-scale rotor.

The test cases selected for the validation exercise are listed in table 1. The rotor shaft angle is $0°$ for all the cases; the trim target is also fixed: $C_T/\sigma = 0.1$ and $\beta_{1,\mathrm{s}} = 0$, $\beta_{1,\mathrm{c}} = 0$ (tip path plane normal to the shaft); the wind tunnel velocity V_{wt} varies in the range 10-40 m/s.

For all the presented simulations the *ROSITA* solver was run in parallel on 72 processors. The simulations took 5 to 10 *ROSITA*/*MBDyn* coupling cycles to converge, depending on the operating conditions, but it generally takes longer for low wind speeds. At each coupling cycle *ROSITA* was run performing 2000 pseudo-time iterations at CFL=2.0 when $V_{\mathrm{wt}} = 10\,\mathrm{m/s}$ and at CFL=5.0 for all the other speeds; the cycle computational time was 10 hours (wall clock). The time consumed by *MBDyn* at each cycle is roughly 5 minutes and it is therefore negligible.

The first comparison regards the measured and computed harmonics of the control and hinge angles, shown in figure 8. The average pitch (figure 8(a)) compares well for wind tunnel (WT) speeds below 20 m/s, while the WT and CFD curves exhibit a roughly constant offset for the higher speeds. Here the behaviour of the WT curve seems not realistic, the sudden increment at $V_{\mathrm{wt}} = 20\,\mathrm{m/s}$ being more likely due to a problem in the measuring instrumentation. The WT and CFD curves for the first harmonics of the pitch angle (figures 8(b)-8(c)) are instead in good agreement over the whole speed range.

The computed coning angle (figure 8(d)) is higher than the measured one. It is however influenced by the inertial properties of the blade, which were not exactly known for the model blade and were only estimated. The curves for the CFD and WT first harmonics of the flap angle are close to zero for all the speeds (figures 8(e)-8(f)), since that was the imposed trim condition.

For what concerns the lead-lag angle, the CFD and WT average value have similar behavior but slightly different absolute values (figure 8(g)). The CFD and WT lead-lad angle first harmonics (figures 8(h)-8(i)) have a high percentage difference but, nonetheless, they are both small in value for all the wind tunnel speeds. The observed discrepancy are in any case not surprising because the damping properties of the lead-lad hinge of the model rotor are not available and they were only guessed within the *MBDyn* model.

The normalized torque coefficient is compared with experimental data in figure 9. The agreement is satisfactory over the whole speed range V_{wt} = 10-40 m/s. It is therefore inferred that the proposed method is suitable to account for the WT interference on the rotor flow.

A final comparison is done against the PIV field data collected for the low speed cases TC1-TC3. The leftmost subfigure of figures 10-12 report the computed in-plane velocity in the PIV plane for considered test cases, the PIV window extension being indicated with a black rectangle. The PIV section is positioned 600 mm away from the of the wind tunnel vertical symmetry plane. The other two subfigures show, respectively, the CFD in-plane velocity and the measured in-plane velocity in the PIV window region. For the TC1 case the agreement is fairly good, the average velocity magnitude having similar value, but the direction of the flow is different, with the measured velocity vector field inclined more downward. The TC2 case is more interesting since the rotor wake is passing through the PIV window. The agreement between the computed and measured field is good: the predicted wake position is nearly the same as the observed one and the velocity magnitude in the computed wake is only slightly lower, probably due to the numerical dissipation. Also for the TC3 case the numerical results compare well with the experiment, both in term of velocity magnitude and flow direction.

It is possible then to conclude that the results achieved with the coupled AD method compare positively with the experimental measurements, thus representing a good compromise between the quality of results and the computational effort.

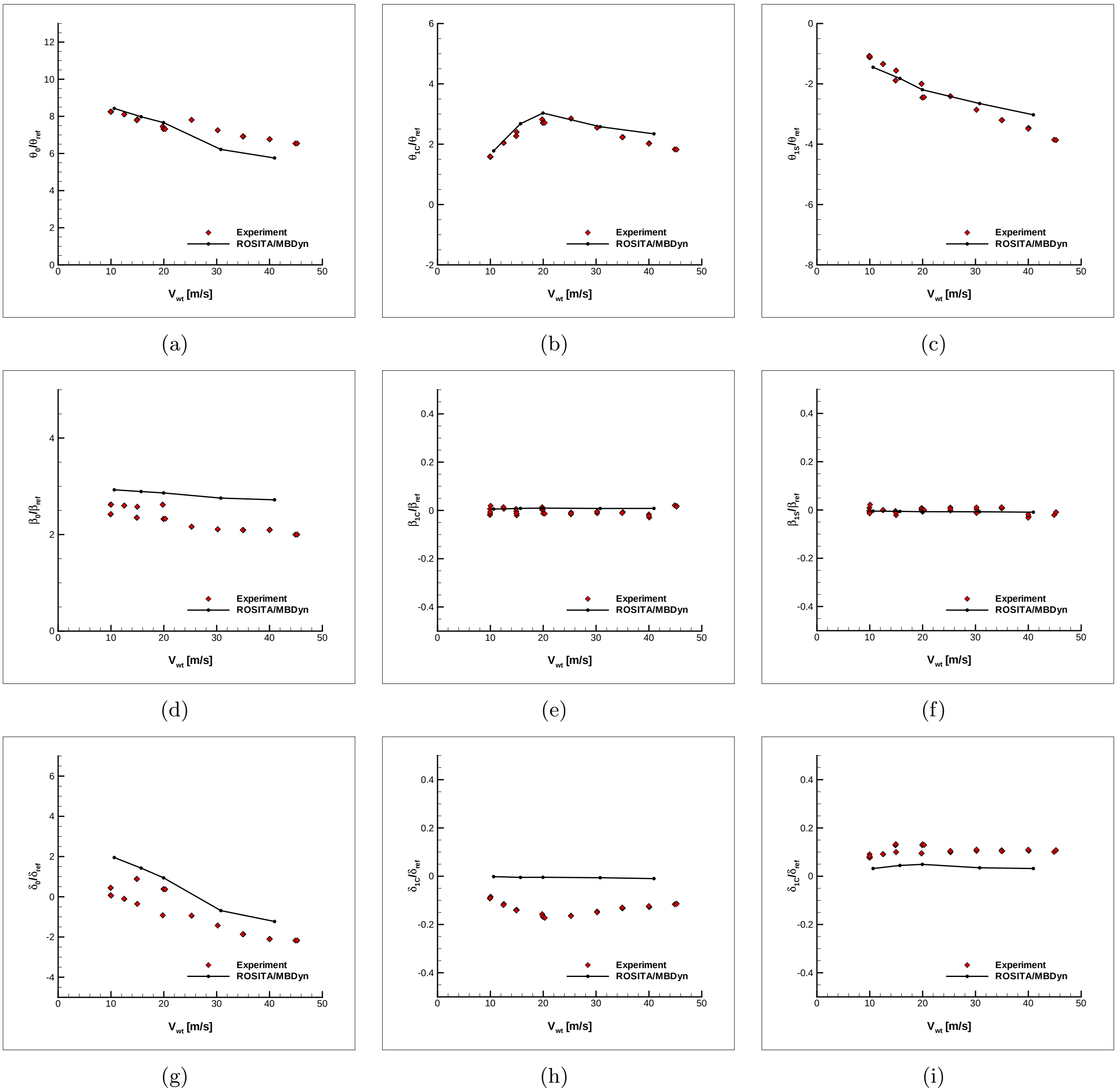

Figure 8: Comparison between measured and computed normalized values of the hinge angle harmonics for the test cases TC1-TC5: (a)-(c) pitch angle, (d)-(f) flap angle, (g)-(i) lead-lag angle.

6 Conclusions

A loosely coupled CSD/CFD method, based on a steady AD model and fully accounting for the rotor dynamics, has been presented, which allows for the calculation of the time-averaged trimmed rotor flow in any kind of aerodynamic environment. The method has been validated by comparing with experimental data the numerical simulation of a model-scale rotor, operating in a wind tunnel with open test section. The achieved agreement in terms of control angles and torque coefficient can be considered satisfactory.

The proposed method represents a computationally efficient alternative to full-rotor trimmed simulations, when the time-averaging assumption may be adopted.

Aknowledgements: this work has been carried out in the framework of Project WITCH (WInd Tunnel Correction metHodology for model rotor tests), funded by AWPARC. The Authors wish to thank G. Campanardi, G. Gibertini and D. Grassi

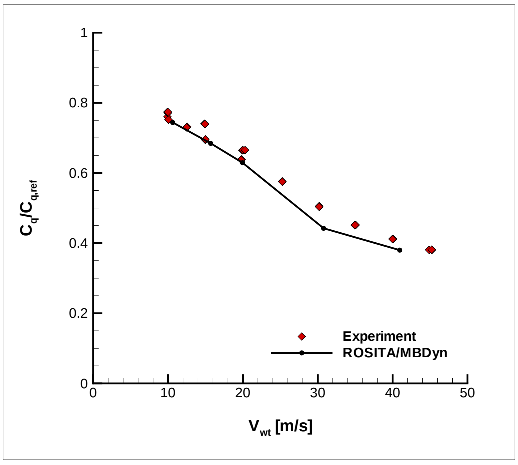

Figure 9: Comparison between measured and computed values of the normalized torque coefficient for the test cases TC1-TC5.

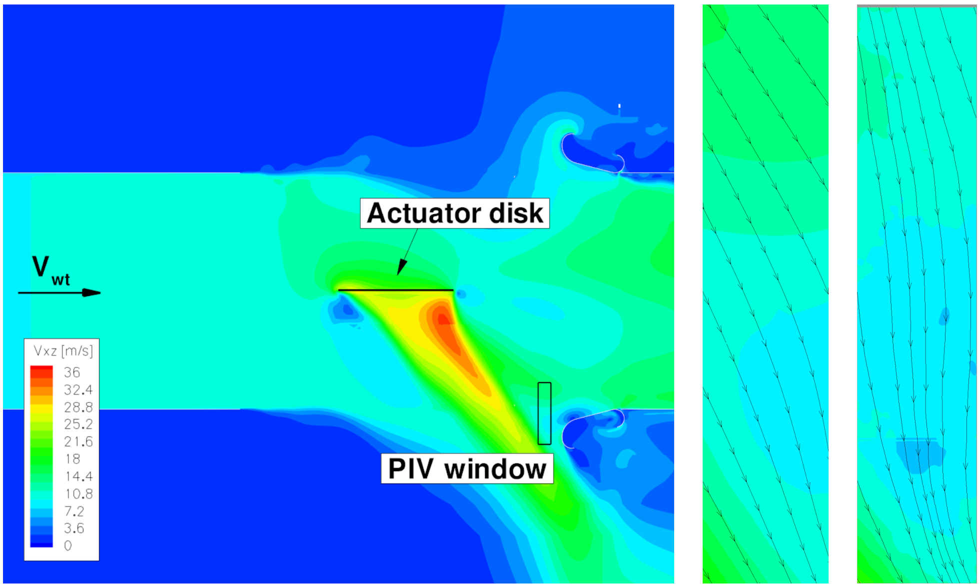

(a) CFD (b) CFD (c) PIV

Figure 10: Comparison between measured and computed velocity field for TC1.

for providing the PIV data and G. Crosta and A. Verna for providing the load and control data of the AW rotor.

References

[1] D.L. Whitfield and A. Jameson. Three-dimensional Euler equation simulation of propeller-wing interaction in transonic flow. In 21st *AIAA Aerospace Sciences Meeting, Reno, NV. AIAA 83-0236*, 1983.

[2] F. Le Chuiton. Actuator disc modelling for helicopter rotors. *Aerospace Science and Technology*, 8:285–297, 2004.

[3] I. Fejtek and L. Roberts. Navier-Stokes Computation of Wing/Rotor Interaction for a Tilt Rotor in Hover. In 29th *AIAA Aerospace Sciences Meeting, Reno, NV. AIAA 91-0707*, 1991.

[4] M.S. Chaffin and J.D. Berry. Navier-Stokes Simulation of a Rotor Using a Distributed Pressure Disk Method. In *American Helicopter Society* 51st *Annual Forum Proceedings*, 1995. Fort Worth, TX.

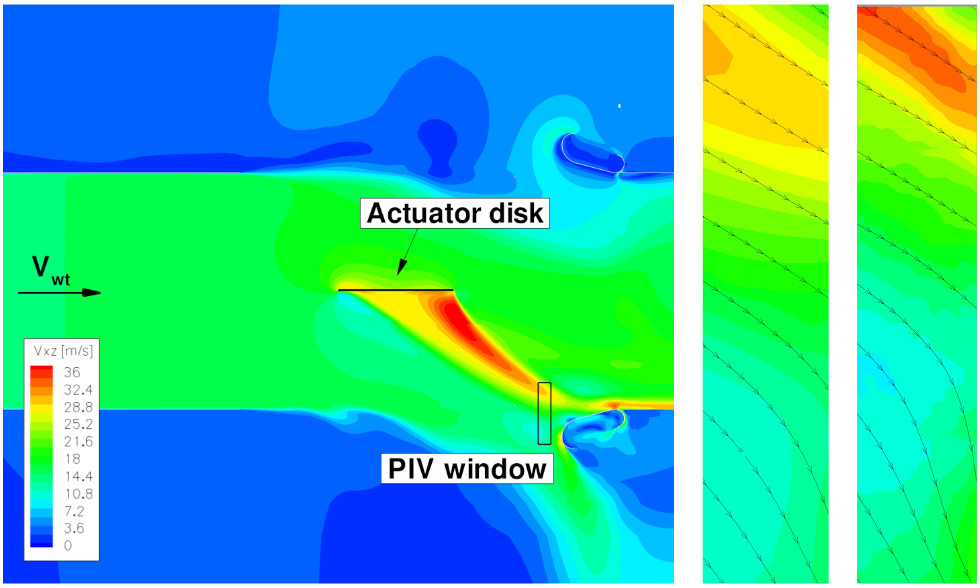

(a) CFD (b) CFD (c) PIV

Figure 11: Comparison between measured and computed velocity field for TC2.

[5] J.-K. Lee and O.J. Kwon. Predicting Aerodinamic Rotor-Fuselage Interactions by Using Unstructured Meshes. *Trans. Japan Soc. Aero. Space Sci.*, 44:208–216, 2002.

[6] S.M. Ruffin and J.-D. Lee. Rotorcraft Flow Field Prediction Accuracy and Efficiency using a Cartesian Grid Framework. *Int. J. of Mathematical Models and Methods in Applied Sciences*, 3:246–255, 2009.

[7] R.G. Rajagopalan and S.R. Mathur. Three Dimensional Analysis of a Rotor in Forward Flight. *Journal of the American Helicopter Society*, 38:14–25, 1993.

[8] L.A. Zori and R.G. Rajagopalan. Navier-Stokes Calculations of Rotor-Airframe Interaction in Forward Flight. *Journal of the American Helicopter Society*, 40(2):57–67, 1995.

[9] N. Bettschart. Rotor Fuselage Interaction: Euler and Navier-Stokes Computations with an Actuator Disk. In *American Helicopter Society* 55st *Annual Forum Proceedings*, 1999. Montreal, Canada.

[10] D.M. O'Brien Jr. and M.J. Smith. Analysis of Rotor Fuselage Interactions Using Various Rotor Models. In 43rd *AIAA Aerospace Sciences Meeting, Reno, NV. AIAA 2005-0468*, 2005.

[11] R. Schweikhard. Actuator Disk for Helicopter Rotors in an Unstructured Flow Solver. *Journal of the American Helicopter Society*, 52:58–68, 2007.

[12] D.M. O'Brien Jr., M.E. Calvert, and S.L. Butler. An examination of engine effects on helicopter aeromechanics. In *AHS Specialist's Conference on Aeromechanics, San Francisco, CA, Jan. 23-25*, 2008.

[13] N. Hariharan, L.N. Sankar, J. Russel, and P. Chen. Numerical simulation of the fuselage-rotor interaction phenomenon. In 34th *AIAA Aerospace Science Meeting, Reno, NV. AIAA 96-0672*, 1996.

[14] H. Tadghighi. Simulation of Rotor-Body Interactional Aerodynamics: An Unsteady Rotor Source Distributed Disk Model. In *American Helicopter Society* 57th *Annual Forum Proceedings*, 2001. Washington, DC.

[15] D.D. Boyd Jr. and R.W. Barnwell. Rotor-Fuselage Interactional Aerodynamics: An Unsteady Rotor Model. In *American Helicopter Society* 54th *Annual Forum Proceedings*, 1998. Washington, DC.

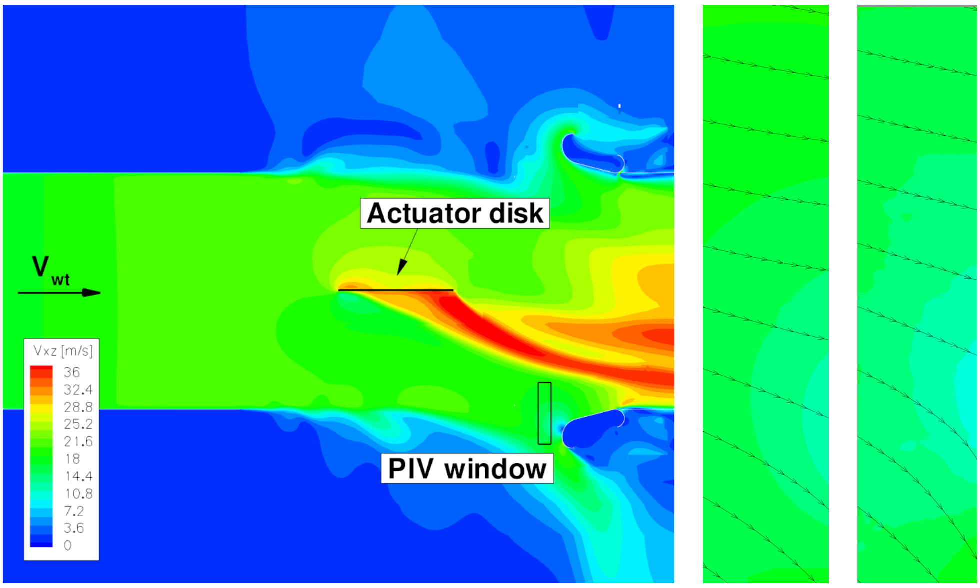

(a) CFD (b) CFD (c) PIV

Figure 12: Comparison between measured and computed velocity field for TC3.

[16] N. Troldborg, J. N. Sorensen, and R. Mikkelsen. Numerical simulation of wake characteristics of a wind turbine in uniform flow. *Wind Energy*, 13:86–99, 2010.

[17] Mbdyn - multibody dynamics http://www.aero.polimi.it/mbdyn/.

[18] M. Biava. *RANS computations of rotor/fuselage unsteady interactional aerodynamics*. PhD thesis, Dipartimento di Ingegneria Aerospaziale, Politecnico di Milano, 2007.

[19] M. Biava, W. Khier, and L. Vigevano. CFD prediction of air flow past a full helicopter configuration. *Aerospace Science and Technology*, 19:3–18, 2012.

[20] P.R. Spalart and S.R. Allmaras. One equation model for aerodynamic flows. In 30^{th} *AIAA Aerospace Science Meeting, Reno, NV. AIAA 92-0439*, 1992.

[21] P.L. Roe. Approximate Riemann Solvers, Parameter Vectors and Difference Schemes. *Journal of Computational Physics*, 43:357–372, 1981.

[22] V. Venkatakrishnan. On the accuracy of limiters and convergence to steady state solutions. In 31^{st} *AIAA Aerospace Sciences Meeting, Reno, NV. AIAA 93-0880*, 1993.

[23] A. Jameson. Time dependent calculations using multigrid with applications to unsteady flows past airfoils and wings. In 10^{th} *AIAA Computational Fluid Dynamics Conference, Honolulu, HI. AIAA 91-1596*, 1991.

[24] E. Turkel, R. Radespiel, and N. Kroll. Assessment of preconditioning methods for multidimensional aerodynamics. *Computers & Fluids*, 6:613–634, 1997.

[25] G. Chesshire and W.D. Henshaw. Composite overlapping meshes for the solution of partial differential equations. *Journal of Computational Physics*, 90:1–64, 1990.

[26] G. Ghiringhelli, P. Masarati, P. Mantegazza, and M.W. Nixon. Multi-body analysis of a tiltrotor configuration. *Nonlinear Dynamics*, 19:333–357, 1999.

[27] D.A. Peters, M. Chouchane, and M. Fulton. Helicopter Trim with Flap-Lag-Torsion and Stall by an Optimized Control. *Journal of Guidance, Control and Dynamics*, 13:824–834, 1990.

[28] M. Biava, G. Campanardi, G. Gibertini, D. grassi, L. Vigevano, and A. Zanotti. Wind tunnel open section characterization for rotorcraft tests. In 38^{th} *European Rotorcraft Forum, Amsterdam, The Netherlands*, 2012.